LBL-30867
UC-402

Lawrence Berkeley Laboratory

UNIVERSITY OF CALIFORNIA

Environmental Research Program

1990 Annual Report

Applied Science Division

April 1992

LOAN COPY
Circulates
for 4 weeks
Bldg. 50 Library.
LBL-30867
Copy 2

Please note name change:

Effective September 1, 1991, the name of the Applied Science Division was changed to *Energy & Environment Division.* Addresses and telephone numbers for the Division remain unchanged.

Available to DOE and DOE Contractors from
Office of Scientific and Technical Information
P.O. Box 62, Oak Ridge, TN 37831
Prices available from (615) 576-8401, FTS 626-8401

Available to the public from
National Technical Information Service
U.S. Department of Commerce
5285 Port Royal Road, Springfield, VA 22161

Prepared for the U.S. Department of Energy under Contract No. DE-AC03-76SF00098

DISCLAIMER

This document was prepared as an account of work sponsored by the United States Government. While this document is believed to contain correct information, neither the United States Government nor any agency thereof, nor the Regents of the University of California, nor any of their employees, makes any warranty, express or implied, or assumes any legal responsibility for the accuracy, completeness, or usefulness of any information, apparatus, product, or process disclosed, or represents that its use would not infringe privately owned rights. Reference herein to any specific commercial product, process, or service by its trade name, trademark, manufacturer, or otherwise, does not necessarily constitute or imply its endorsement, recommendation, or favoring by the United States Government or any agency thereof, or the Regents of the University of California. The views and opinions of authors expressed herein do not necessarily state or reflect those of the United States Government or any agency thereof or the Regents of the University of California.

Environmental Research Program
1990 Annual Report

Tihomir Novakov, *Program Leader*

Applied Science Division
Lawrence Berkeley Laboratory
University of California
Berkeley, California 94720
(510) 486-5001

LBL-30867

Environmental Research Program Staff

Tihomir Novakov, ***Program Leader***

Susan Anderson
Frank Asaro
Ann H. Bambauer
W. Henry Benner
Nancy Brown
Johnny Chang
Shih-Ger Chang
Robert Cheng
Susan Chung
Raymond Dod
Ofodike Ezekoye
Drazen Fabris
Carlos Fernandezpello
Charles Fleischmann
Stephanie Frolich
Ian Fry
Robert Giauque
Gloria Gill
Ralph Greif
Anthony Hansen
John Harte
Erika Hoffman
Kenneth Hom
Minh Hua
Gary Hubbard
Nori Hudson
Margaret Huflejt
Franklin Hurlbut
Catherine Koshland
Angela Lai
Dan Landy
David Littlejohn
David Liu
Jau-Huai Lu
Donald Lucas
Robert Macey
John Maguire
Samuel Markowitz
Richard Martin
Andrew J. Maxson
Rolf Mehlhorn
Harvey Michaels
Helen Michel
Katherine Moore
Mario Moronne
Mark Nicholas
Tihomir Novakov
Antoni Oppenheim
Lester Packer
Patrick Pagni
Mark Paige
Andrew Papp
Ahmed Rashed
Chang Woo Rhee
Robert Risebrough
Carlos Rivera-Carpio
Ruben Rosso
Jennifer Rutherford
Robert Sawyer
Frank Schipperijn
Richard Schmidt
Richard Schneider
Ian Shepherd
Linda Sindelar
Martyn Smith
David Steward
Lawrence Talbot
Chang-Lin Tien
Derek Watry
Gillian Wild
Robert Williamson
Linda Wroth

Contents

INTRODUCTION ..... *i*

FLUE-GAS CHEMISTRY

LBL PhoSNOX Process for Cleanup of Flue Gas 1
Kinetics of the Oxidation of Aqueous SO_2 by NO_2 and O_2 2
Modeling of Aqueous Scrubber Solutions 3
Properties of the Salts of Nitrogen-Sulfur Compounds 5
New Metal Chelates for Nitric Oxide Removal from Flue Gas 6

COMBUSTION

Combustion Chemistry 7
Combustion Fluid Mechanics 9
Thermal Destruction of Toxic Compounds 11
Controlled Combustion 12

ATMOSPHERIC AEROSOLS

Reaction of NO_2 With Laboratory Clouds 13
Formation of Particulate Nitrate by the Reaction Between NO_2, Water Vapor, and Laboratory Aerosols 14
In Situ Measurement of Cloud Integrated Backscattering Coefficient with a Modified Nephelometer 16
Aerosol Particle Technology 17

MEMBRANE BIOENERGETICS

Free Radicals, Heavy Metal Toxicity, and Antioxidants 18
Biological Oxidations, Free Radicals, and Oxygen Toxicity 19

ECOLOGICAL SYSTEMS

Assessing Ecotoxicological and Genotoxic Effects in Environmental Management 20

Introduction

The objective of the Enviromental Research Program is to contribute to the understanding of the formation, mitigation, transport, transformation, and effects of energy-related pollutants on all compartments of the environment. This multidisciplinary program includes both basic and applied research in physics, chemistry, engineering, ecology, and biology, as well as research and development of advanced technologies for pollutant abatement and destruction, efficient combustion, and new methods of detection and analysis of different contaminants. The Program's Annual Report contains summaries of research performed during 1990 in the areas of combustion, flue-gas chemistry, atmospheric aerosols, ecological systems, membrane bioenergetics, and analytical chemistry.

The *Combustion Group* studies complex combustion processes by acquiring a fundamental understanding of the physical and chemical processes that determine the combustion efficiency, formation, and emissions of species from these processes. The *Flue-Gas Chemistry Group* is engaged in research whose aim is to help develop new processes for simultaneous SO_2 and NO_x removal. The *Atmospheric Aerosols Group* studies atmospheric chemical processes in the laboratory and in the field, and develops novel methods for individual particle characterization. New activities have been initiated by the *Ecological Systems Group* to develop means of predicting the toxicity of contaminants in aquatic and terrestrial ecosystems. The *Membrane Bioenergetics Group* studies the effects of chemically reactive compounds on biological systems. The main emphases in *Analytical Chemistry* have continued to be in the area of asteroid impacts and mass extinctions.

FLUE-GAS CHEMISTRY

LBL PhoSNOX Process for Cleanup of Flue Gas

T.Q. Li and S.G. Chang

Previously we discovered that aqueous emulsion of yellow phosphorus (P_4) was effective in removing NO from flue gas in a simple wet scrubber. P_4 reacts with O_2 in flue gas to produce ozone. Ozone can rapidly oxidize insoluble NO to NO_2, which is soluble and can be removed by alkaline scrubbing liquors. This process has been named LBL PhoSNOX.

During the past year, we have demonstrated that LBL PhoSNOX is capable of highly efficient NO removal (greater than 95%) from flue gas using a 20 cfm bench-scale scrubber with NO concentrations ranging from those found in flue gas of a coal-fired boiler (600 ppm in the case of an old pulverized-coal boiler or 300 ppm in a new p-c boiler) to those in a natural gas-fired boiler (<100 ppm), as shown in Figure 1. We have also shown that the utilization of P_4 (P/NO ratio) is more effective when dilute P_4 concentration is employed (Figure 2). However, the NO removal efficiency may not reach a desirable value if the P_4 concentration is too dilute. Consequently, one has to maintain enough P_4 concentration in liquors to achieve a desirable NO removal efficiency, but not too much P_4 so that the waste of P_4 can be avoided.

When this process was used for combined removal of NO_x and SO_2 from flue gas, the fate of P_4, NO_x, and SO_2 in this process was examined. A majority of P_4 was oxidized to H_3PO_4, which can be recovered for commercial use. We found that the presence of HSO_3^-/SO_3^{2-} in scrubbing liquors at a concentration typical in wet FGD systems (>1 mM) would cause most of the NO_2 to react via

$$NO_2 + SO_3^{2-}/HSO_3^- \rightarrow NO_2^- + SO_3^-/HSO_3$$

Only a small fraction of NO_2 is removed via a dissolution pathway

$$2\,NO_2 + H_2O \rightarrow HNO_2 + HNO_3$$

Consequently, most of the dissolved NO_2 is initially converted to HNO_2. The interaction of HNO_2 and HSO_3^- forms various nitrogen-sulfur compounds; under most scrubbing conditions the major species is hydroxylamine disulfonate (HADS)

$$HNO_2 + 2\,HSO_3^- \rightarrow HON(SO_3)_2^{2-} + H_2O$$

HADS can be removed from scrubbing liquors through precipitation as a potassium salt. This can be decomposed at ~100 C to form N_2, NH_3, and K_2SO_4. The latter reagent can be recycled. An alternate route for treating nitrogen-sulfur compounds is by way of hydrolysis under acidic conditions to form NH_4HSO_4. The absorbed SO_2 is eventually converted to sulfate which can be precipitated as a gypsum byproduct.

George Lee of Bechtel corporation has recently updated a cost evaluation of this process based on a new conceptual integrated process configuration we derived. The results revealed that the LBL PhoSNOX process compared favorably to the SCR (selective catalytic reduction) process when high NO_x removal efficiency (greater than 90%) was required, and was comparable to a urea-injection process in achieving a 50% removal efficiency. A proposal to conduct pilot plant (3MW) tests of this process involving Bechtel Corp., FMC, and LBL has been submitted to the State of Illinois and the U.S. Department of Energy.

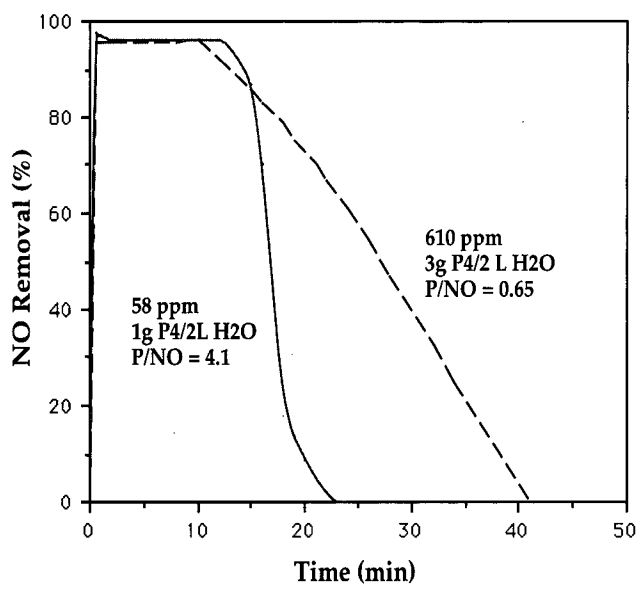

Figure 1

Figure 1. The removal efficiency of NO for NO concentrations of 58 and 610 ppm in a simulated flue gas.

References

Chang SG, Liu DK. Removal of nitrogen and sulphur oxides from waste gas using a phosphorus/alkali emulsion. *Nature* 1990; 343: 151-153.

Liu DK, Shen DX, Chang SG. Removal of NO_x and SO_2 from flue gas using aqueous emulsions of yellow phosphorus and alkali. *Environ. Sci. & Technol.* 1991; 25: 55-60.

Lee GC, Shen DX, Littlejohn D, Chang SG. The use of wet limestone systems for combined removal of SO_2 and NO_x from flue gas. EPRI report (also published as Lawrence Berkeley Laboratory Report No. LBL-27595) presented at the 1990 SO_2 Control Symposium, sponsored by EPA/EPRI, May 8-11, 1990, New Orleans, Louisiana.

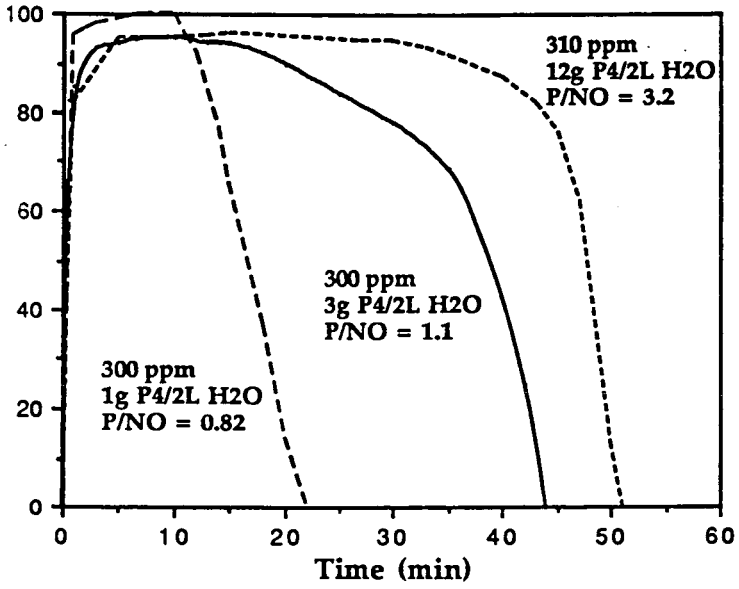

Figure 2. The dependence of stoichiometric ratio (P/NO) on the concentration of yellow phosphorus in spraying liquors.

Kinetics of the Oxidation of Aqueous SO_2 by NO_2 and O_2

Y.Z. Wang, D. Littlejohn, and S.G. Chang

The LBL PhosNO_x process uses yellow phosphorus to induce the oxidation of relatively insoluble nitric oxide (NO) to nitrogen dioxide (NO_2). Nitrogen dioxide reacts with both dissolved sulfur dioxide and water. The kinetics of these reactions have not been extensively studied, and more information is needed to properly understand processes used to remove NO_2.

The reaction was investigated by rapidly flowing gas mixtures containing low concentrations of NO_2 and O_2 over well-stirred solutions of sulfite or bisulfite ions. The concentrations of the species in the solution were measured periodically using Raman spectrometry or ion chromatography. The gas mixture was sampled before and after the reaction cell with a chemiluminescent NO_x analyzer to insure that no more than 10% of the NO_2 was absorbed. The reaction was studied as a function of NO_2 concentration, O_2 concentration, SO_3^{2-}concentration, and temperature.

The reactions involved in the reaction of NO_2 with dissolved SO_2 are listed below.

(1) $2\,NO_2 + H_2O \rightarrow NO_3^- + NO_2^- + 2H^+$

(2) $NO_2 + SO_3^{2-} \rightarrow NO_2^- + SO_3^{\cdot -}$

(3) $SO_3^{\cdot\cdot} + SO_3^{\cdot -} \rightarrow S_2O_6^{2-}$

(4) $SO_3^{\cdot\cdot} + SO_3^{\cdot -} \rightarrow SO_3 + SO_3^{2-}$

(5) $SO_3 + H_2O \rightarrow 2\,H^+ + SO_4^{2-}$

(6) $NO_2^- + 2\,HSO_3^- \rightarrow HON(SO_3^-)_2 + OH^-$

(7) $HON(SO_3^-)_2 + HSO_3^- \rightarrow N(SO_3^-)_3 + H_2O$
$NH(SO_3^-) + HSO_4^-$

(8) $HON(SO_3^-)_2 + H_2O \rightarrow HONHSO_3 + HSO_4^-$

By operating at pH > 9, it is possible to avoid significant involvement of reactions 6 - 8. There have been several studies of the dissolution of NO_2 in water, as well as the reaction of NO_2 with sulfite and bisulfite. The sum of the rate constants for reactions 3 and 4 has been reported. Using this value with our measurements of the concentrations of $S_2O_6^{2-}$

and SO_4^{2-} produced, we can assign values to the rate constants k_3 and k_4. At 25°C, $k_3 = 3.8 \times 10^8$ liter/mole-second and $k_4 = 7.2 \times 1\ 0^8$ liter/mole-second.

When oxygen is present in the gas mixture, several additional reactions become important:

(9) $SO_3^{\cdot} + O_8 \rightarrow SO_5^{\cdot -}$

(10) $SO_5^{\cdot\cdot} + SO_3^{2-} \rightarrow SO_3^{\cdot -} + SO_5^{2-}$

(11) $SO_5^{2-} + SO_3^{2-} \rightarrow 2\ SO_{42}^{-}$

Oxygen has the effect of the amount of sulfate (SO_4^{2-}) produced relative to the amount of dithionate produced ($S_2O_6^{2-}$). Other effects are under study.

Reference

Hayon E, Treinin A, Wilf J. Electronic Spectra, Photochemistry, and Autoxidation Mechanism of the Sulfite-Bisulfite-Pyrosulfite Systems. The SO_2^-, SO_3^-, SO_4^-, and SO_5^- Radicals. *J. Am. Chem. Soc.* 1972; 94: 47.

Modeling of Aqueous Scrubber Solutions

D. Littlejohn and S.G. Chang

The NO_x and SO_2 absorbed by aqueous scrubbing liquors can react in solution to form nitrogen-sulfur compounds. The nitrogen-sulfur compounds such as HADS (hydroxyamido-disulfonate, or hydroxyimidodisulfate), HAMS (hydroxyamidomonosulfonate, or hydroxysulfamate), ATS (aminetrisulfonate, or nitridotrisulfate), and ADS (aminedisulfonate, or imidodisulfate) are fairly soluble in solution and, if discharged in wastewater from the flue gas desulfurization (FGD) scrubbing liquor, could require additional treatment prior to release. It would be advantageous to determine the scrubber operating conditions in which production of the N-S compounds and N_2O are minimized. There are a large number of reactions occurring in scrubbing liquors in which both sulfur oxyanions ($SO_2 \cdot aq$, HSO_3^-, SO_3^{2-}, $S_2O_5^{2-}$, SO_4^{2-}) and nitrogen oxyanions (HNO_2, NO_2^-, NO_3^-) are present.

To model these reactions, we adapted a modeling program that has been used in air pollution studies. The reactions are symbolically entered into the program along with the rate constants and initial conditions. The output is in the form of concentrations *vs* time for the species of interest. The package runs on a Macintosh computer with a Fortran 77 compiler. The reactions[1] can be broken down into gas absorption, NO_x and SO_x inter-conversions, production and interconversion of nitrogen-sulfur (N-S) compounds, and decomposition of N-S compounds. The systems were modeled to determine the fraction of absorbed nitrogen oxides that are converted to N-S compounds and N_2O. The conditions of the modeled scrubbing liquor that were varied include pH, temperature, and L/G.

The modeling routine was used to simulate two basic types of wet limestone FGD systems. In the first type of system is the standard wet limestone FGD system, with co-current flow, widely in use in the U.S. Several modifications of this basic design were studied. One modification considered is the oxidation of NO to more-soluble NO_2 in the gas phase, as with the Phosnox process. Other modifications were a counter-current flow absorber, in which the sprayed droplets of scrubbing liquor flow in an opposing direction to the flow of the flue gas; and a metal chelate system with enhanced NO solubility. The second type of system investigated is based on the Chiyoda CT-121 process, which bubbles the gas through the scrubbing liquor with additional oxidizing air.

From the calculations we can compare the fraction of absorbed NO_x converted into NO_2^-, NO_3^-, N_2O, and N-S compounds. The reaction products for the scrubber systems are compared in the Figure. The system with enhanced NO solubility produces the largest quantity of N_2O of the systems compared, as might be expected. The simulation of the scrubbing system in which most of the NO is oxidized to NO_2 in the gas phase (as with the Phosnox system) produces essentially no N_2O. Since considerable amounts of NO_2^- are produced, N-S compound formation is relatively high. The simulation of the Chiyoda system generated somewhat lower concentrations of N-S compounds than the other systems. This is primarily due to the forced oxidation of S(IV), which is incorporated into the system design.

The results of our simulations indicate that lower temperatures minimize production of both N_2O and nitrogen-sulfur compounds. Maintaining the scrubbing liquor above pH 5.5 will help minimize N-S compound formation. Solution pH has little effect on N_2O formation. Rapid oxidation of S(IV) to sulfate not only minimizes $CaSO_3$ formation, but reduces the rates of the dissolved NO_x with S(IV) reactions that produce N-S compounds. At these conditions, the Chiyoda CT-121 process appears to be capable of reducing NO_x conversion to N-S compounds. The Phosnox process should be capable of nearly eliminating N_2O production. Systems which enhance NO solubility may have problems with N_2O formation, although the metal chelate system used can exert strong influence on the solution chemistry.

In summary, the simulations of scrubbing liquor chemistry provide quantitative results of the effects of scrubber conditions on the production of nitrogen-containing products. The accuracy of the calculations are limited by current

knowledge of the solution kinetics of the reactive species in scrubbing liquor and by the ability to model heterogeneous processes (such as dissolution and formation of solid particles) and free radical processes. Without a kinetic model, it is very difficult to predict the quantities of N_2O and N-S compounds that will be formed in scrubbing liquors. This investigation indicates a number of areas in which additional research is needed. A better understanding of NO_2 aqueous chemistry is needed, especially for the reactions involved with the conversion of $NO_2(aq)$ to NO_2^- and NO_3^-. The S(IV) oxidation process is still poorly understood. Further studies of N-S compound chemistry are needed.

Reference

Chang SG, Littlejohn D, Lin NH. Flue gas desulfurization. In: Hudson JL, Rochelle GT, Eds., *ACS Symposium Series 188*. American Chemical Society, Washington, DC, 1982; 127-152.

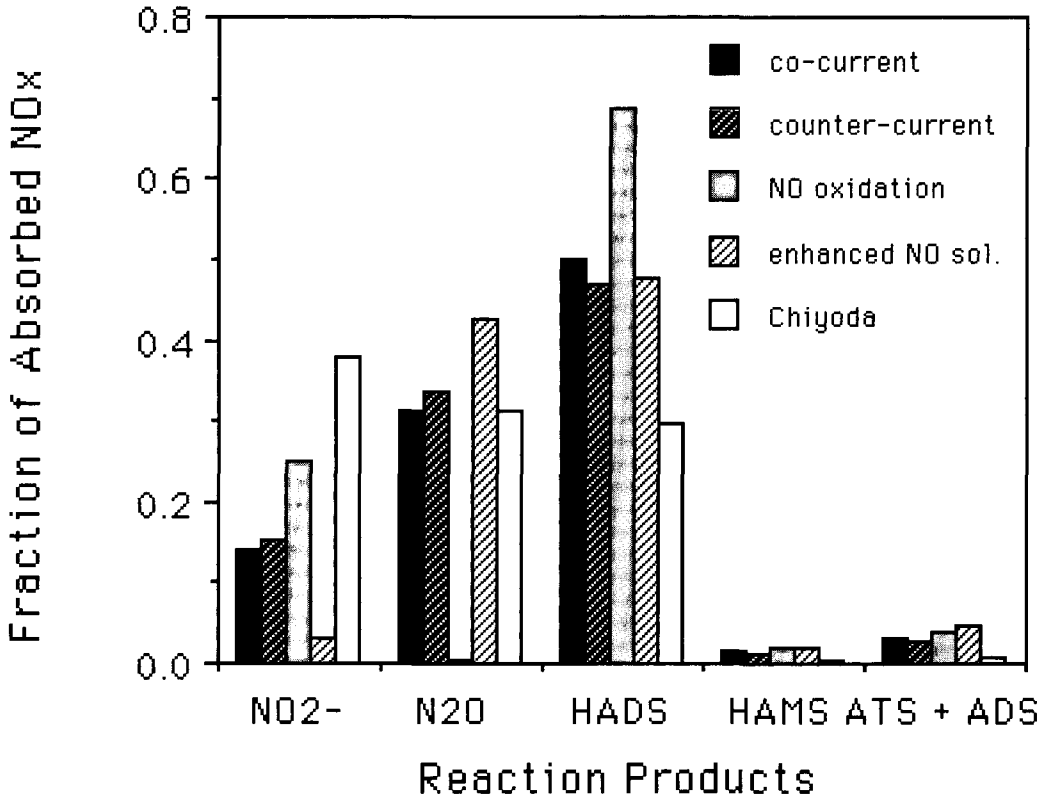

Figure. Comparison of products generated by different scrubber processes.

Properties of the Salts of Nitrogen-Sulfur Compounds

D. Littlejohn and S.G. Chang

The nitrogen-sulfur compounds hydroxyimidodisulfate (HADS), hydroxysulfamate (HAMS), nitridotrisulfate (ATS), and imidodisulfate (ADS) are formed by the reaction of nitrite ion with bisulfite ion in aqueous solution. Hydroxylamine and sulfamate are formed by the hydrolysis of HAMS and ADS, respectively. The solubility of these compounds must be known to develop methods of precipitating them from solutions used to remove NO_x and SO_2 from flue gas.

A saturated solution of each of the compounds was prepared by adding excess salt to a small volume of water in a controlled temperature bath and steadily stirring the solution. After allowing sufficient time for saturation to occur, the solution was sampled to determine the concentration of the compound. Measurements were generally made over a temperature range of 0 to 50°C.

The expressions for the solubility of the potassium salts as a function of temperature are listed below (T is in units of °C).

HADS: [HADS] (M) $= 0.433 + 0.0454 \times T$
HAMS: [HAMS] (M) $= 0.0694 + 8.09 \times 10^{-3} \times T$
ATS: [ATS] (M) $= 3.83 \times 10^{-3} + 4.13 \times 10^{-4} \times T$
ADS(2-)[a]: [ADS^{2-}] (M) $= 0.025 + 9.4 \times 10^{-4} \times T + 4.2 \times 10^{-5} \times T^2$ [b]
ADS(3-)[a]: [ADS^{3-}] (M) $= 0.6 + 0.3 \times T$ [c]

[a] The pK_a for ADS is 8.5 at $\mu = 1$
[b] The values above 30°C are somewhat uncertain. This is the current best fit to the data.
[c] Tentative results. Further measurements are in progress.

Potassium sulfamate is much more soluble than the potassium salts of the other nitrogen-sulfur compounds.

The calcium salts of the nitrogen-sulfur compounds appear to be significantly more soluble than the corresponding potassium salts. Work is currently in progress to isolate pure calcium salts of the nitrogen-sulfur compounds. Listed below are estimates for solubilities of some of the calcium salts.

[ATS] $\geq$ 1 M at 20°C
[ADS^{2-}] $\geq$ 2 M at 20°C
[Ca^{2+}sulfamate] = 4 to 5 M over the temperature range of 15 to 30°C.

Information on the thermal degradation of nitrogen-sulfur compounds is needed so that they can be treated after removal from scrubbing solutions. The thermal decomposition of ATS, ADS, sulfamic acid, and hydroxylamine has been reported in the literature. Our measurements indicate that ATS decomposes to ADS and $KHSO_4$ at 80°C. At 450°C, it decomposes to yield the following products.[1]

$$2N(SO_3^-)_3 \rightarrow 2S_2O_7^{2-} + SO_4^{2-} + S + N_2$$

This decomposition appears to involve the intermediate $(NSO_2^-)_3$.

Both the (2-) and (3-) charge states of ADS are fairly stable. The (2-) ADS salt decomposes with the following overall reaction:

$$3HN(SO_3^-)_2^{2-} \rightarrow 3SO_4^{2-} + 3SO_2 + N_2 + NH_3.$$

The decomposition of the (3-) ADS salt involves a similar intermediate, $(NSO_2)_3^{3-}$, but forms a different product set.

$$2N(SO_3)_2^{3-} \rightarrow 3SO_4^{2-} + S + N_2$$

This decompostion occurs above 200°C and becomes rapid above 300°C.

Neither hydroxylamine nor its sulfonated derivatives appear to be very stable at elevated temperatures. Limited studies in our laboratory on HADS at 80°C suggest that it decomposes as follows:

$$HON(SO_3K)_2 \cdot H_2O \rightarrow NH_2OH + K_2S_2O_7$$

While the decompostion of HAMS has not been studied, we can speculate from the behavior of other hydroxylamine derivatives that it decomposes to yield the sulfate salt and gaseous species such as NH_3, N_2 and H_2O.

Reference

Parent Y. Decompositions thermiques des imides sulfurique et carbonique Schema reactionnel; extension à $HN(SO_2F)_2$ et $N(SO_3)_3^3$. *Rev. Chim. Miner.* 1984, 21: 183.

New Metal Chelates for Nitric Oxide Removal from Flue Gas

J.B. Zheng, D.K. Liu and S.G. Chang

The use of Fe(II) complexes of SH-containing ligands for NO removal in wet flue gas clean-up system has been studied. In the first approach, commercially available ligands were used. We found the resulting Fe(II) complexes of cysteamine, dithiooxalate (DTO), *meso*-2,3-dimercaptosuccinate (DMS), and 2,3-dimercapto-1-propansulfonate (DMPS) can be used to remove NO from flue gas in a wet scrubber system. All experiments were carried out at 55°C by bubbling a gaseous mixture of NO (500 ppm), O_2 (5%) and N_2 (balance) into buffered solution containing one of the above Fe(II) complexes. The concentration of NO before and after scrubbing was monitored by a chemiluminescent NO_x analyzer. We found that all the above SH-containing ligands can reduce Fe(III) produced by the reaction of Fe(II) with O_2 in flue gas, thus maintaining adequate concentrations of Fe(II) complexes for NO removal. The NO absorption capacity (as expressed by the number of moles of NO removed per mole of Fe(II) added, or n_{NO}/n_{Fe}) of these Fe(II) additives as a function of scrubber pH was examined. We found that only the NO absorption capacity of Fe(II)(cysteamine)$_2$ was sensitive to pH, with a maximum n_{NO}/n_{Fe} of 0.70 at pH 5.7 ($n_{cysteamine}/n_{Fe} = 4$). Furthermore, the NO absorption capacity increased by 47% in the presence of SO_3^{2-} and HSO_3^- in the Fe(II)(cysteamine)$_2$ scrubbing solution. On the other hand, we found no pH effect on the NO absorption capacities of Fe(II)(DTO)$_2$, Fe(II)(DMPS)$_2$, and Fe(II)(DMS)$_x$ (x = 1 or 2), and the n_{NO}/n_{Fe} ratios were measured to be 0.96 ($n_{DTO}/n_{Fe} = 2$; pH 5.1) and 0.45 ($n_{DMPS}/n_{Fe} = 4$; pH 5.6), and 0.067 ($n_{DMS}/n_{Fe} = 4$; pH 6.1), respectively. In all these systems, both nitrite and nitrate ions were detected in the scrubbing solutions as result of the oxidation of the coordinated NO by O_2. Moreover, in the case of Fe(II)(cysteamine)$_2$, some of the coordinated NO can be reduced by exccess ligand to form mostly N_2 and traces of N_2O. Finally, we found that cysteamine and DMPS can be regenerated from their disulfide forms using various chemical reduction methods, thus making possible the recycling of valuable reagents.

In another approach, new dithiocarbamates and xanthates which resemble ethylenediaminetetraacetic acid (EDTA) in molecular structure are synthesized. The rationale here is to combine the favorable properties of Fe(II)-dithiocarbamates (high NO absorption capacity; little N_2O or dithionate production) with those of Fe(II)-EDTA (fast NO absorption kinetics). An example is a previously unknown dithiocarbamate which we prepared by the reaction between ethylenediaminediacteic acid (EDDA) and carbon disulfide in the presence of sodium hydroxide. The production of the ligand was confirmed by laser Raman spectroscopic studies of the reaction mixtures as well as elemental analysis of the solids subsequently collected. Preliminary NO absorption experiments using a neutral solution containing 0.01 M Fe(II) and ~0.03 M of the dithiocarbamate ligand and a gas mixture containg 500 ppm NO and 5% 0_2 showed a maximum NO absorption efficiency of 51% and a nNO/nFe ratio of 0.47. The n_{NO}/n_{Fe} ratio for Fe(II)-EDTA would be ~0.05 under similar conditions. Another system under investigation is a new xanthate ligand which we prepared by the reaction between hydroxyethylethylenediaminetriacetic acid (HEEDTA) and carbon disulfide. Future efforts will be focused towards a more comprehensive study of the NO absorption mechanism involving these new ligands and the determination of the fate of the absorbed NO and the ligands after the reactions.

Reference

Chang SG, Littlejohn D, Liu DK. Use of ferrous chelates of SH-containing amino acids and peptides for the removal of NO_x and SO_2 from flue gas. *IE&C Research* 1988; 27:2156-2161.

Liu DK, Chang SG. Removal of nitric oxide from flue gas using water-soluble iron(II) dithiocarbamates. *Environ. Sci. Technol.* 1988; 22:1196-1200.

COMBUSTION

Combustion Chemistry

N.J. Brown, J. Chang

Combustion processes are governed by chemical kinetics, energy transfer, transport, fluid mechanics, and the complex interactions among these. Understanding chemical kinetics and energy transfer offers the possibility of better understanding combustion so that it can be controlled. Our recent research has been concerned with the application of functional sensitivity analysis to determine the relation between dynamic observables and the potential-energy surface structure. This has revealed important information about energy transfer processes and reactivity.

In collaboration with Herschel Rabitz of Princeton University, we have continued our research on developing and constructing classical sensitivity maps in diatom-diatom collisions. In preliminary studies, the full-sensitivity maps were quite complex; our particular interest here was in understanding the convergence properties of the full-sensitivity maps, the importance of the higher-order potential terms, and the relation of spatial resolution to complexity and convergence properties.

The case of rotational energy transfer in coplanar collisions of H_2 + HD was selected for study to focus on the development questions in classical functional sensitivity analysis. As in previous studies, the intermolecular diatom-diatom potential was expanded in the angular series

$$V(R, \phi_1, \phi_2) = \Sigma v_{m_1,m_2} \cos(m_1\phi_1 + m_1\phi_2)$$

and the sensitivity to these higher-order (m_1,m_2) terms were of particular interest. We calculated observables (energy transfer quantities from trajectories run on the full potential) and compared these to observables from trajectories run on truncated potentials constructed by adding more (m_1,m_2) terms. A truncated potential with $|m_i| \leq 1$ can transfer energy only between translation and HD rotation. Inclusion of terms up through $|m_i|_{max} = 2$ allows for coupling between all degrees of freedom, and essentially give the correct final energy partitioning of the full potential. Hence, the higher-order terms are clearly not important for describing the dynamics of this system. However, this type of calculation does not tell us how errors in the higher-order terms affect the dynamics and this information would be required if the higher-order terms had to be adjusted to give better agreement with the experiment. Sensitivity analysis provides the latter type of information.

In the sensitivity differential equations, the so-called inhomogeneity vector is the quantity responsible for causing a "perturbation" on the trajectories. In a strictly classical formalism, the inhomogeneity vector is a delta function, and this represents a singularity of classical functional sensitivity analysis. The delta functions must be broadened if the calculation is to be feasible; they are approximated as Gaussians or a particular width. This width parameter affects spatial resolution and convergence and, in a sense, incorporates some of the localization uncertainties of quantum mechanics. The choice of width parameters is determined by two competing factors: 1) by keeping width parameters small, the classical result is more nearly simulated; 2) by increasing the widths, the sensitivity at each point will include contributions from trajectories close to the point so that a smaller total number of trajectories will be required for convergence. We chose the radial width factor to be 0.25 a.u. and the angular width factor to be 0.20 radians. These values were chosen by carefully varying the parameters over a range of values to assure that large-scale structures and symmetry were preserved in the maps, and to approximate closely the classical result. Choosing these two factors determined a resolution factor for identifying significant structure in the observable sensitivities, which in turn places a lower bound on the size (physical extent) of the potential perturbations that we can consider.

The full-sensitivity coefficients were expanded in a series involving radial sensitivity coefficients multiplied by cos $(m_1\phi_1 + m_2\phi_2)$ in analogy with the potential. We also derived an exact expression for planar cuts of the full sensitivities at fixed values of one of the angles, and this was used to directly compute the full sensitivity maps. By comparing results of the two approaches to computing full-sensitivity maps, we could determine the values of m_1 and m_2 for which the sensitivity series was converged. The series was converged for $|m_i| \leq 6$.

Several results emerge from these calculations. Larger values of the width parameter would scale down the importance of the sensitivities to the larger (m_1, m_2) combinations. The defining equation for observable sensitivities must be examined to determine the effect of higher-order terms. This involves integrating the product of the sensitivity with variations in the potential. Specifically, large sensitivity coefficients must accompany sizable potential variations in order to have a large effect on the observables. Many more trajectories are needed to converge the sensitivities than the observables because in calculating the sensitivities, an averaged quantity is resolved into its many components to produce the sensitivity maps. (A paper describing these calculations is in preparation.)

Performed in collaboration with Herschel Rabitz and Robert Wyatt, our current research is concerned with functional sensitivity analysis studies of quantum reactive scattering. We focus initially on the H_3 system and its isotopic analogues: $H + H_2$, $D + H_2$, and $H + D_2$. As an initial effort,

we are calculating sensitivities for collinear $H + H_2$ reactions. The Porter Karplus-2 (PK-2) potential is used in standard test-case calculations for new methods in active scattering and has been used by others for sensitivity analysis using a finite-element approach for reactive scattering calculations to determine quantum sensitivities. We have used the log derivative version of the Kohn variational principle for our reactive scattering calculations and have derived expressions for the sensitivities in this formalism. Our computed sensitivities agree with the earlier results of others.

One objective of the current study is to address a fundamental question in sensitivity analysis: Under what circumstances will the sensitivity analysis tell us where to calculate the higher densities of ab initio points? To answer this question, we calculated the sensitivities with an "incorrect" potential (the (PK-2) surface) and with a more "correct" potential (the Liu, Sietgbahn, Truhlar, and Horowitz (LSTH)potential). The PK-2 surface differs from the LSTH surface in the saddle point region as well as in other regions. Figure 1 shows the sensitivity map of the $P_{00\text{-}Q}$ reactive transition probability at 0.8706 eV for the LSTH surface as a function of the mass scaled coordinates for collinear $H + H_2$. A resonance occurs at this energy and the transition probability has a local minimum value. The sensitivities on the LSTH surface show large structures in the same region of configuration space as those calculated on the PK-2 surface.

We are also exploring a new application of sensitivity analysis. First, we calculate sensitivities for the transition probability for one of the potentials (the nominal potential) and calculate the differences between the nominal potential and the other potential along the collinear geometry. We then use the sensitivity coefficients and the potential variations with the defining equation for the observable sensitivity to calculate the transition probabilities associated with the reactive scattering on the other potential. This works well for energies that are not close to those associated with resonances; we are currently exploring changes in sensitivity behavior for energies close to resonances. We are also performing a type of parametric sensitivity analysis to obtain time delays. Time delays are the duration of quantum resonances and are determined by calculating the energy derivative of the S-matrix.

For FY91 we will compute a collinear rate coefficient from the collinear analogues of the thermal rate equations and will use sensitivity analysis to explore connections between microscopic collision phenomena and macroscopic rate processes. After completing the study of collinear $H + H_2$ reactions, we will perform functional sensitivity analysis studies on the three-dimensional quantum reactive scattering of $H + H_2$, $D + H_2$, and $H + D_2$.

References

Martin RJ, Brown NJ. Nitrous oxide formation and destruction in lean premixed combustions. *Combustion and Flame* 1990; 80: 238-255. (also published as LBL Report No. LBL-27127)

Martin RJ, Brown NJ. Analysis and studies of nitrous oxide chemistry in lean premixed combustion. *Combustion and Flame* 1990; 82: 312-333. (also published as LBL Report No. LBL-27128.

Martin RJ, Lucas D, Brown NJ. Nitrogen species measurement in a flash-ignited combustion system. Extended abstract for the Joint Meeting of the Canadian Combustion Section and the Western States Section of the Combustion Institute; also poster session at the Twenty-Third Symposium (International) on Combustion, 1990. (also published as LBL Report No. LBL-28735)

Brown NJ, Longuemare M. Calculation of rotational energy transfer rates for HD (v = 1) in collisions with thermal HD. *Journal of Chemical Physics* 1990; 93: 2413-2417.

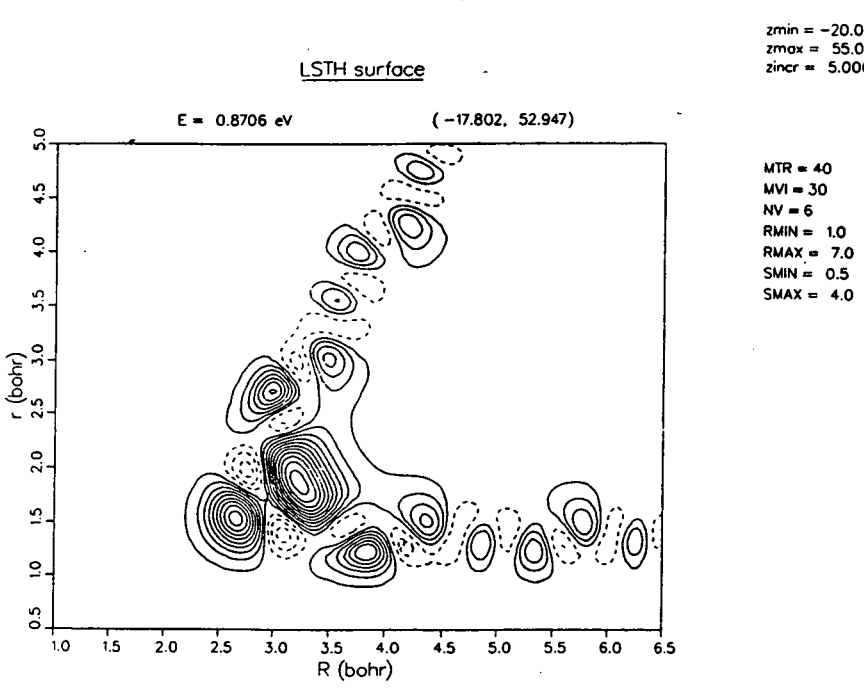

Figure 1. Contour diagram of the functional sensitivity of the P_{00} reactive transition probability for the $H + H_2$ reaction as a function of the mass-scaled coordinates. Dashed lines indicate negative sensitivities.

Combustion Fluid Mechanics

R.K. Cheng, I.G. Shepherd, and L. Talbot

In engines and all types of industrial and domestic burners, combustion takes place predominantly under turbulent flow conditions in order to enhance the overall burning rate. Turbulent combustion processes therefore involve complex interactions between turbulence and flame chemistry which influence both combustion efficiency and the concentrations of by-products such as pollutants in the exhaust. These interactions are characterized by intense fluctuations in temperature, velocity, concentration and pressure. The large range of overlapping temporal and spatial fluctuation scales presents major challenges to the development of turbulent combustion theories capable of predicting burner performance and emission characteristics.

Our research is directed towards the understanding of the fundamental physical processes controlling turbulence-combustion interactions. Such knowledge is basic to the development of theories which can address a variety of practical combustion problems. The approach is to investigate turbulent combustion in laboratory burners designed to simulate the salient flow features of various combustor designs by the use of laser diagnostics which measure scalar and velocity fluctuations and statistical cross-correlations. At present, our experiments are focussed on studying flame conditions with fluid mechanical time scales much larger than those of chemical reactions. Simplified theoretical treatment of these flames is possible and several models have been developed which need experimental validation and verification. The experimental data have been used for comparison with model predictions in addition to determining the effects of turbulence intensity on burning rates.

For our laboratory flames, the flame sheet or laminar flamelet model provides a good physical description of the turbulence/flame interaction. Chemical reactions are confined within thin flame sheets, typically less than 1 mm, which separate the burned products from the unburned reactants. The scalar and velocity properties can then be specified by the burned and the unburned states because the statistical contributions of the flame sheet or burning states to the time mean properties are small. One of the most significant implications of this model is that the turbulent burning rate can be described in terms of the increase in the flame surface area caused by turbulence induced wrinkling and corrugation.

As reported in FY90, we have developed a high speed cine tomographic technique to investigate the flame surface area and the related scalar scales. Tomography is a flow visualization method which produces instantaneous, two-dimensional (2-D), cross-sectional images of the flame sheet. Our high speed movies show for the first time temporal behavior of premixed and non-premixed turbulent flames of several flame configurations under various flow and chemical conditions. On each frame the flame sheet is delineated by a wrinkled flame boundary which can be digitized and analyzed by a video image processing system. The most convenient method to compute the wrinkle scales of the flame boundaries is by means of fractal analysis. These movies provide a large amount of usable data, and so we have been able to report the only set of results to date which can be considered to be statistically stable. Previous analyses reported by other investigators have usually been based on a small amount of data. Many issues concerning the convergence requirements of fractal analysis of flame boundaries have not been adequately addressed.

The application of fractal analysis to turbulent premixed flame fronts is a relatively new technique and the careful investigation of the effects of the various experimental parameters on fractal calculations is an important task in the evaluation of the method. We have taken advantage of the large amount of flame boundary data provided by the cine records and conducted an evaluation of the effects of spatial resolution, digitization noise, and the requirements for statistical convergence in the fractal analysis of premixed turbulent flame boundaries.

Fractal analysis is a means of characterizing the size of an irregular object in terms of measurement scale which vary over several orders of magnitude. For our two-dimensional flame boundaries the length, L, varies with the measurement scale, E. If a power law relationship exists between the length and the measurement scales, the flame boundaries are considered to be fractalized. There are three fractal parameters which characterize these boundaries: the fractal dimension, D, represents the rate at which the length increases with the measuring scale, i.e. the slope of the line arrange of a log-log fractal plot. The inner and outer cut-off measurement scales correspond to the smallest and largest flame wrinkles which are the upper and lower limits of the linear region. In order to determine the fractal dimension, a clear delineation of the fractal range is necessary (Fig. 1).

Our investigation shows that for typical experimental data this can only be achieved by the statistical averaging of at least 25 realizations because the fractal parameters derived from single images can be widely scattered. To investigate the effects of reduced resolution, the 512-by-512 digitized flame boundaries were averaged to simulate those obtained with 256-by-256, 128-by-128 and 64-by-64 pixel resolutions (Fig. 2). The influence of the digitization noise,

which arises because the digitized flame boundaries are characterized by discrete steps, was addressed by smoothing. The fractal plots derived from a set of 200 flame boundaries for the different spatial resolutions with and without smoothing were compared. We have found that the inner cut-off can be obscured by digitization noise and by insufficient spatial resolution. The effects of digitization noise on E_1, can be removed by smoothing the flame boundaries only when the spatial resolution is sufficient. If the spatial resolution is too low, however, smoothing of the flame edges produces plausible but erroneous results. The requirements necessary to resolve the outer cutoff are analogous to those for large-scale turbulent fluctuations; the record size, i.e. the field of view of the tomograph, has to be larger than the largest significant scale, i.e., E_0. This also implies that a consistent record size, i.e. flame boundary length, will improve the accuracy of E_0.

We have also evaluated the merits of different fractal analysis methods for flame studies. In principle, the fractal parameters can be derived from fractal plots of either L versus E or N versus E. L is the physical length of the flame boundary measured at given E and L = EN. Our results show that due to the limiting conditions of the fractal plots it is more difficult to identify the fractal range on the N versus E representation. The L versus E plot, therefore, provides a more sensitive means of extracting the fractal parameters from experimental data. This investigation has helped to identify the convergence requirement and set the standard for fractal analysis of flame boundaries. Our investigation of the characteristics of flame boundaries was extended to the determination of the local flame front curvature from the tomographic images. Curvature of a flame front, induced by either turbulence or inherent laminar instabilities, is known to effect the propagation rate of the flame front and hence the total burning rate. Various methods have been proposed for the determination of the curvature, e.g. Fourier descriptor analysis, but they proved unsuccessful with our data so we devised a 'least mean square' technique using a circle as the fitting function. The incorporation of an efficient convergence algorithm (Marquand minimization) greatly improved the method. Probability density functions of local flame front curvature were generated which exhibited marked asymmetry in shape due to significant 'cusping' of the flame towards the burnt gases. The mean curvature, however, was very close to zero for all the cases studied.

Premixed flame front instabilities arising from a variety of causes (including body forces, hydrodynamics and diffusional effects) are an area of extensive current study. We have investigated a premixed hydrogen/air flame which is unstable (with a Lewis number less than one) in a turbulent flow and compared it, by means of local curvature and fractal analysis, with a stable methane/air flame. A much higher fractal dimension and burning rate was found in the former case and also a significantly higher probability of large curvatures. This finding indicates an important aspect of turbulence/combustion interactions which requires further study.

We have also progressed in our numerical work in simulating the dynamics of the wrinkled flame sheet. The method we are adopting to follow the evolution of a flame front whose speed depends on the local curvature is based on work by Professor J. Sethian of the U.C. Berkeley Department of Mathematics. The new algorithms he has developed approximate the equations of motion of propagating fronts with curvature-dependent speed, i.e., Propagation of Surfaces under Curvature (PSC) schemes. The PSC algorithms accurately compute the curvature along the flame, avoid numerical instability, and naturally handle topological merging and breaking during the evolution of the flame front.

To apply these algorithms to a turbulent v-flame, it has been necessary to couple them with a vortex dynamics approach to describe both the turbulence in the oncoming stream and the vorticity production by the flame itself, and a volume production model to represent combustion heat release. The PSC algorithms are employed to propagate the flame and the flame is advected by the underlying flow field. Conditioned and unconditioned mean and RMS values of the two velocity components and the Reynolds stress deduced from the numerical results compare well with experimental data. Flame wrinkling, in response to the incoming flow vortices used to simulate free stream turbulence intensity, increases in amplitude as the turbulence is increased, also in accord with experiment. The thickness of the flame brush also increases. When, in an extreme case, a single strong vortex is injected into the incoming flow, a sharp cusp develops and propagates along the flame, as has been observed in our experiments. The notable effects of the flame-generated vorticity are twofold: one is to increase the turbulence level in the burnt mixture as is verified by experiments, and the other is to decrease the flame angle by the acceleration of the centerline velocity. Comparisons of the conditioned and unconditioned data are used to differentiate the contribution of the flame to "flame generated turbulence" from that of intermittent measurement in the reactants and products.

Thermal Destruction of Toxic Compounds

D. Lucas, R. F. Sawyer, C. P. Koshland, E. M. Fisher, R. Cervera, C. McEnally, M. Thompson, and S. Lee

The reduction or elimination of toxic wastes from our environment is a problem that must be attacked. The latest EPA figures estimate that 4.57 billion pounds of toxic chemicals were released into the environment in 1988. While there is a public mandate for action, the methods of choice for obtaining a better environment are embroiled in considerable controversy. Reducing the amount of hazardous materials that are produced and used is an obvious step, but it also should be apparent that source reduction will not eliminate the need for safe, effective means of disposal of compounds that are toxic or hazardous.

One method being used to treat both hazardous and conventional wastes is incineration. Proper incineration can convert a broad range of hazardous chemicals into compounds that are much less toxic and easier to control, and significantly reduce the amount of landfill needed for disposal. Incineration is not a panacea, however, and the continued and increased use of thermal destruction techniques hinges upon the public acceptance of combustion as a safe, relatively non-polluting technique.

Our research focuses on the combustion of chlorinated hydrocarbons under non-ideal conditions, and the detection of these species. By themselves chlorinated hydrocarbons form a major class of hazardous wastes, and incomplete combustion of these wastes can lead to emissions of the compound being destroyed, and the formation of hazardous reaction products (products of incomplete combustion, or PICs).

We are studying the thermal destruction of chlorinated hydrocarbons in a laboratory scale turbulent flow reactor, with products monitored by FTIR/long path spectroscopy. We have studied the injection of methyl chloride, ethyl chloride, and 1,1,1-trichloroethane vapor into the post flame gases of a lean propane/air flame. A wide variety of products have been observed, including phosgene, vinyl chloride, and dichloroethylene, all of which are *more* toxic than the original material injected.

In certain cases we have found that intermediates can be formed which are more stable than the original chlorinated species, and that the emissions of CO, often used as an indicator of incomplete combustion, do not follow emissions of more toxic species.

Modeling of the chemical kinetics has provided evidence that not all of the important products and mechanisms responsible for byproduct formation have been identified. For example, vinyl chloride was not expected to be formed from ethyl chloride. To explain these results, we developed a mechanism which accounts for isomeric C_2 chlorinated hydrocarbons. With this mechanism, we found that ethyl chloride is destroyed by HCl elimination, and by Cl abstracting an H atom. The radical attack produces two species, CH_2Cl_2 and CH_3CHCl, which can decompose unimolecularly to form C_2H_4 and C_2H_3Cl.

We are also developing new *in situ* diagnostic methods for the detection of chlorinated hydrocarbons using photofragmentation-laser induced fluorescence. A 193-nm ArF excimer laser is used to fragment the chlorine-containing species into smaller pieces. The fragments are then detected by their characteristic fluorescence. We have observed C, C_2, CH, Cl_2, HCl, and CCl fragments from CCl_4, CH_3Cl, and C_2H_5Cl. The CCl fragment is observed only when a molecule containing a carbon-chlorine bond is photolyzed; it thus can be used a detector for unburned chlorinated hydrocarbons. The CCl radical has two transitions at 236 and 278 nm that we will probe using a dye laser system to excite fluorescence and increase the sensitivity of the method.

References

Fisher EM, Koshland CP. Numerical Simulation of the Thermal Destruction of Some Chlorinated C_1 and C_2 Hydrocarbons. *J. Air Waste Mgmt. Assoc.* 1990; 40: 10.

Fisher EM, Koshland CP, Hall MJ, Sawyer RF, Lucas D. Experimental and Numerical Study of the Thermal Destruction of C_2H_5Cl. *23rd Symposium (International) on Combustion* (in press, 1991).

Hall MJ, Lucas D, Koshland CP. Measuring Chlorinated Hydrocarbons in Combustion Using FTIR Spectroscopy. *Environ. Sci. Technol.* (in press, 1991).

Koshland CP, Fisher EM, Lucas D, Sawyer RF. Thermal Destruction of Some Chlorinated C_1 and C_2 Hydrocarbons. Presented at the 1990 AIChE Annual Meeting, November, 1990, and submitted to *Combust. Sci. Technol.*

Lucas D, McEnally C, Sawyer RF, Koshland CP. Detection of Chlorinated Hydrocarbons by Photofragmentation. Presentation at the *23rd Symposium (International) on Combustion*, August, 1990.

Controlled Combustion

K. Hom, J. A. Maxson, A. K. Oppenheim, and H. E. Stewart

Current technological standards treat combustion chambers for prime movers solely as sources of power, without much attention being given to their performance as chemical reactors. Consequently, these chambers have a relatively unconstrained tendency to produce air pollutants. In the automotive industry, for example, the strategy adopted world-wide for reducing pollutant emissions has been to reduce their concentrations by chemical processing of combustion products in the exhaust system. In contrast, the basic purpose of our studies is to provide a scientific basis for *controlling the combustion process* in order to reduce formation of pollutants. Notably, the same means benefit fuel economy as well as engine tolerance to a wide variety of fuels.

Our ultimate goal is to advance the technology of internal combustion engines. For this purpose, we must not only understand systems and processes currently in use; we must also explore and assess other concepts. After more than a decade of studying the fundamentals of ignition and combustion engines—of particular relevance to internal combustion engines—we are now beginning to develop and study new concepts.

Thus, having published studies demonstrating the influence of dilution upon auto-ignition, we have concentrated on developing effective means for executing the combustion process. The major function of these methods is to modify the progress of evolution of exothermic energy and its deposition in the working substance, so as to render it externally controllable by a microprocessor. The particular mode we are exploring in this connection is associated with the use of turbulent plumes of pulsed jets (i.e., pulsed-jet combustion, PJC).

The primary purpose of our preliminary investigation of PJC was to compare the performance of this mode of combustion to that of a conventional spark-ignited flame traversing the charge (FTC). Using a highly diluted air/fuel mixture as the working substance, we conducted experiments in a constant-volume vessel of a size representative of typical automotive engines in the course of the exothermic process of combustion. Our results showed the advantages of PJC over FTC in initiating and carrying out the combustion process. In particular, they lead to the following conclusions:

• *PJC can initiate and promote the combustion process in extremely lean media*, i.e., in a mixture whose equivalence ratio is 0.45. (Under identical conditions, spark ignition requires equivalence ratios under 0.65 in order to initiate combustion.)

• *The effectiveness of a PJC-initiated process is superior to that of FTC.* PJC rate is about twice as fast and the heat transfer losses to surroundings significantly lower than with FTC, so that the maximum pressure attained in the combustion chamber is about 10% higher.

Future studies will attempt to determine the mechanical and chemical structure of PJC, establishing its properties as a means of executing combustion under microprocessor control so as to restrain formation of pollutants.

ATMOSPHERIC AEROSOLS

Reaction of NO_2 with Laboratory Clouds

A. Bambauer, B. Brantner, and T. Novakov

Gas-liquid interactions are not viewed as surface chemical processes but considered as a sequence of mass transport processes followed by aqueous-phase homogeneous reactions. The mechanisms and rate equations used to describe aqueous reactions are derived from bulk solution measurements under the explicit assumption that these are directly applicable to dispersed systems such as clouds and fogs.

The question of the equivalency of bulk and dispersed (high surface to volume) systems is beginning to attract the attention of the atmospheric chemistry community for a very important reason: if bulk versus dispersed differences are demonstrated for specific reactions and found to be important, then atmospheric chemistry models will have to be appropriately modified. NO_2 is expected to react slowly with cloud water according to the equation

$$2NO_2\,(g) + H_2O(l) \rightarrow 2H^+ + NO_2^- + NO_3^-,$$

Our work has produced results that are clearly inconsistent with this picture of NO_2 chemistry:

- Nitrate forms rapidly when NO_2 reacts with a laboratory cloud.
- The nitrate concentrations associated with subsaturated NaCl aerosol, and especially with cloud drops, substantially exceed the maximum level expected from scavenging the HNO_3 impurity present in the NO_2 supply; i.e., there results a net production of aerosol or cloud water nitrate.
- The composition of cloud drops exposed to NO_2 is radically different from bulk water exposed to NO_2 from the same source. (Bulk water through which NO_2 is passed by bubbling contains equimolar concentrations of NO_3^- and NO_2, as expected from the well-known disproportionation reaction $2NO_2(g) + H_2O(l) \rightarrow 2H^+ + NO_2^- + NO_3^-$; in contrast, cloud water contains only NO_3^- and essentially no NO_2^-.)

Our results on NO_2^- cloud reactions were obtained by using a concurrent-flow atmospheric pressure/cloud chamber, where a humidified aerosol stream mixes with cold dilution air to produce the cloud by cooling the mixture below the resultant dew point. Depending on the flow rates, particle concentrations, and the inlet stream dew point, clouds with liquid water content (LWC) between 0.2 and 3.0 g/m^3 can be produced. Cloud drops were collected by an impactor located about 30 cm below the chamber top. The impactor cutoff was such that it collected only cloud drops but freely passed aerosol particles. In the presence of the cloud, particles that passed through the impactor were defined as interstitial aerosols and were collected on a Teflon backup filter located downstream from the impactor. As in aerosol experiments, the gaseous products were collected in two deionized water bubblers in series, placed behind the aerosol filters. The NO_2 supply and chemical analyses were the same as in the aerosol experiments.

From the very first experiments with this system, it became clear that the composition of cloud drops exposed to NO_2 in the chamber radically differs from the composition of bulk water into which NO_2 from the same source is absorbed. Passing NO_2 (diluted in dry air or NO_2) through a bubbler containing deionized water resulted in equimolar amounts of nitrate and nitrite, as expected from the well-known disproportionation reaction

$$2NO_2(g) + H_2O(l) \rightarrow NO_3^- + NO_2^- + 2H^+.$$

The analyses of impactor samples showed that nitrate was the only species present when the cloud was reacted with NO_2 in the range 0.5-3 ppm. Nitrite concentrations were below detection except at the lowest NO_2 concentrations (0.2-0.5 ppm), where trace amounts of nitrite ions were detected. This result is definitely different from what is expected from the well-known process of NO_2 dissolution in bulk water and is an indication that the NO_2 reaction in dispersed and bulk systems is fundamentally different.

The chamber nitrate concentrations, measured with 3 ppm NO_2 concentrations and cloud LWC from ~0.5 to 2.7 g/m^3, varied from about 3 to 8 $\mu mol\ m^{-3}$ (or from about 2.2 to 6% of the input NO_2). No correlation between LWC and nitrate was observed. All nitrate concentrations are above 2 $\mu mol/m^3$, i.e., the value is the expected maximum contribution of nitric acid impurity (1.5% of 134 $\mu mol\ m^{-3}\ NO_2$). We therefore conclude that there is a net production of nitrate in the laboratory cloud (which is greater than in the aerosol experiments) and that the LWC of this cloud is not the main factor governing nitrate formation.

A potentially significant insight into the nitrate formation process was obtained by examining the relationship between the Na^+ and NO_3^- concentrations in the collected cloud water. In contrast to our results with NaCl aerosol experiments, where the filter-collected Na^+ concentrations were essentially constant in all runs for constant atomizer NaCl solutions, in cloud experiments a significant variability in the Na^+ concentration was observed. Because the atomizer output was found to be constant over long periods, the Na^+ variability is probably due to the details of NaCl aerosol incorporation into the cloud drops and the removal of large drops by gravitational settling. In two series of experiments, two atomizer solutions with NaCl concentrations of 5 and 10 g/L were used. It was found that NO_3^- correlates extremely

well with Na^+ for both atomizer solutions but with two distinctly different slopes. For the same Na^+ concentrations, two times higher NO_3^- concentrations are observed for 5 g/L than for 10 g/L atomizer solutions.

This striking result demonstrates the influence of the CCN size on nitrate production. For constant atomizer flow conditions, lower NaCl concentrations result in smaller aerosol size because the atomizer drop size is not affected by the solution concentration. However, because of different solute concentrations in the atomizer drops, the aerosol size will be different after the drops are evaporated. To achieve the same mass concentrations, the number concentration of particles produced with 5 g/L will be two times higher than with 10 g/L. It is therefore possible that the parameter controlling NO_3^- formation is the number concentration (and not the mass) of the NaCl aerosol, or of cloud drops nucleated on these particles. Another manifestation of the role of this parameter is that the H^+ concentrations in cloud water correlate with the Na^+ concentrations. It is of interest to note that the cloud drops in these experiments were quite acidic (average pH~3.0) in spite of the fact that the NO_3^- to Na^+ ratio in these runs is 1:1, as expected for neutral $NaNO_3$.

All cloud experiments described above were performed with constant NO_2 concentrations of 3 ppm (134 μmol/m^3). We have also carried out a series of runs with lower NO_2 concentrations. Over the NO_2 range (0.2-3 ppm), the nitrate shows a linear dependence on NO_2 concentration (r = 0.92).

We have formulated two tentative hypotheses to explain our results. The first is that the observed dispersed vs. bulk differences are due to an intrinsic, possibly surface chemical, property of high surface-to-volume aqueous systems. The second is that the uptake of NO_2 and its conversion to nitrate ion in a dispersed aqueous system is strongly enhanced by trace amounts of nitric acid adsorbed on subsaturated aerosols, cloud drops, or aerosol particles that serve as cloud condensation nuclei.

Formation of Particulate Nitrate by the Reaction Between NO_2, Water Vapor, and Laboratory Aerosols

B. Brantner and T. Novakov

Our research on the reactions of NO_2 with NaCl aerosols and cloud drops (see following contribution) was intended to reconcile some of the discrepancies between published results on NO_2-solid and NO_2-aerosol NaCl systems, and to extend the experiments to cloud drops nucleated on NaCl aerosol.

We propose the existence of at least two pathways for nitrate formation by an NO_2-NaCl reaction: a humidity-dependent process involving gas-phase nitric acid formation and its subsequent reaction with NaCl to produce $NaNO_3$, and a humidity-independent pathway resulting in $NaNO_3$ and gaseous NOCl. We may add to these a possible heterogeneous surface chemical mechanism suggested by our results.

NO_2-NaCl and Na_2SO_4 aerosol reactions were studied in an aerosol/flow chamber. The aerosol's effective transit time was ~3 min. The chamber was operated in a relative humidity range of 20%-99%. NaCl and Na_2SO_4 particles were generated by atomizing NaCl and Na_2SO_4 solutions. The atomizer output droplets were dried in two annular silica gel diffusion driers before introduction into the chamber inlet manifold. The chamber concentration of the NaCl aerosols was maintained between 0.46 to 0.62 mg/m^3. The aerosol sampling train consisted of a Teflon filter and, in some experiments, a backup nylon filter. Aerosol particles were collected on the Teflon filter, while the nylon filter was used in some runs to determine the concentration of gaseous nitric acid at the top of the chamber. The gaseous products were collected in two deionized water bubblers in series, placed behind the aerosol filters. Water-extracted Teflon and nylon filters and bubbler water were analyzed for anions (Cl^-, NO_2^-, NO_3^-) and cations (Na^+, NH_4^+) by ion chromatography.

Commercial NO_2 was introduced through a separate Teflon-lined inlet tube close to the bottom of the chamber, where it was mixed with the dilution air to attain a desired chamber concentration between 0.2 and 3 ppm. Because commercial NO_2 cylinders usually contain small amounts of nitric acid as an impurity, we determined the concentration level of the HNO_3 impurity by a well-established method for quantitative determination of nitric acid by nylon filters. The upper limit for the HNO_3 impurity was found to be 1.5% of the input nitrogen dioxide. We refer to this impurity as "primary" nitric acid to distinguish it from the acid produced in the chamber. Several distinct features became evident from these experiments. In contrast to aerosol Na^+ concentrations, which remain constant throughout the r.h. range, Cl^- concentrations show a marked decrease at relative humidities between ~50% and 80%. Filter-collected aerosol nitrate concentrations increase monotonically with r.h. up to the NaCl deliquescence point (75%) and remain essentially constant above this point. No NO_2^- ion was detected in these aerosol samples. Essentially no gas-phase nitric acid was

collected in these runs on nylon filters placed behind Teflon filters.

That the reaction or reactions involved in nitrate formation and chloride loss occur during the aerosol residence in the chamber and not on the filter during sampling was demonstrated by first collecting the NaCl aerosol samples without NO_2 in the chamber at low r.h. and then exposing these precollected NaCl samples to NO_2 at different relative humidities. Only traces of nitrate and no loss of chloride were observed on these filters. Runs with blank filters with NO_2 in the absence of aerosol in the chamber showed essentially no nitrate, irrespective of r.h.

Identical experiments were performed using Na_2SO_4 aerosol instead of NaCl, with identical Na^+ concentrations in the chamber. The results of these experiments are shown in the Figure, where the nitrate concentrations associated with the two aerosols are plotted against r.h. (The NaCl data points in this figure are the averages corresponding to discrete r.h. intervals.) The difference in nitrate concentrations measured with NaCl and Na_2SO_4 is obvious. Very low nitrate concentrations were detected below 60% r.h. with sodium sulfate aerosol. However, above 75% the nitrate levels detected with both aerosols are similar. These results suggest that nitrate formation below ~75% r.h. is related to a property specific to the NaCl aerosol.

Before further discussions of the data, we examine the effect of the primary nitric acid found as an impurity in the NO_2 supply. If we conservatively assume this HNO_3 (1.5% of cylinder NO_2) is scavenged by the aerosol with 100% efficiency (and assuming no loss on chamber walls), it would contribute a constant nitrate concentration of ~2 μmol/m^3, as indicated by the horizontal dashed line in Fig. 1. Low-humidity nitrate on NaCl aerosol could therefore be due to the nitric acid impurity. However, the nitrate concentrations of NaCl aerosol at r.h. above ~50% are higher than could be explained by the HNO_3 impurity. We note that the low-humidity nitrate on the Na_2SO_4 aerosol is almost an order of magnitude lower than the 2 μmol/m^3 value, implying that the Na_2SO_4 particles scavenge HNO_3 less efficiently than NaCl particles.

There are at least two possible reasons for the differences observed with these two aerosol compounds. The first is that the nitrate is produced almost entirely by the humidity-dependent NOCl pathway below the NaCl deliquescence point. The other reason may be the occurrence of surface chemical reactions related to the distinct differences in the water vapor uptake mechanism by NaCl and Na_2SO_4. NaCl takes up water only in the unbound state. At the deliquescence point (NaCl = 75% r.h.), a saturated aqueous solution is formed. Therefore, there is always intermolecularly unbound, adsorbed water available on a sodium chloride aerosol, even at relative humidities below deliquescence. Sodium sulfate, however, chemically binds up to 12 molecules of water (water of hydration) into its crystal structure before it reaches the deliquescence point, above which the aerosol growth is similar to that of NaCl. This clearly distinguishes the two aerosol species by their free water content. Consequently, if the nitrate formation mechanism requires adsorbed, but not chemically bound, water, then such a mechanism will be more efficient with NaCl aerosol. The hydration properties of the NaCl aerosol also explain the chloride loss dependence on relative humidity. HCl will be degassed while the NaCl aerosol is relatively dry but will hydrolyze and remain in solution above the deliquescence point. These results indicate that at elevated humidities there is a net production of nitrate (most likely nitric acid) in the chamber.

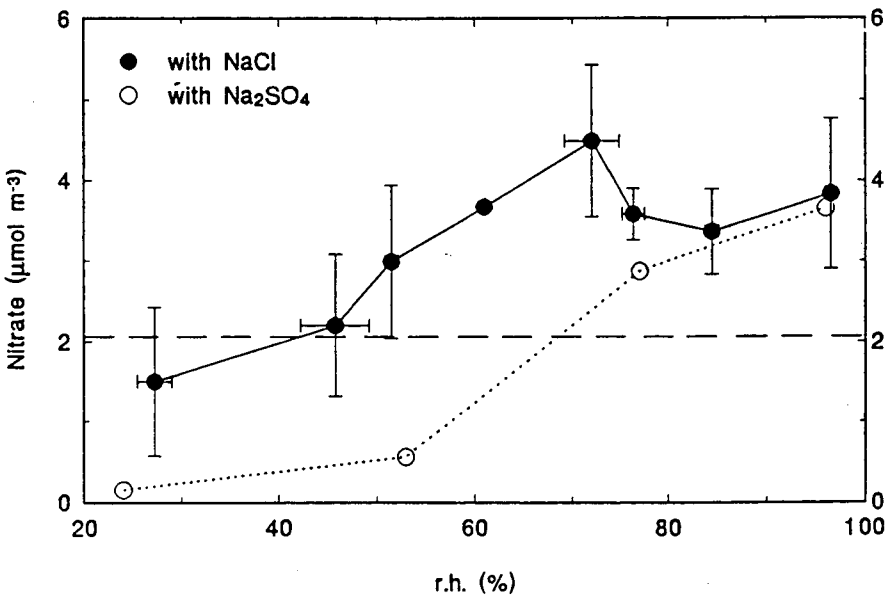

Figure. Aerosol nitrate concentration determined from experiments with NaCl and Na_2SO_4 particles plotted against relative humidity. The values for r.h. and nitrate (with NaCl) represent the mean (n = 3-5) concentrations ± s.d. for discrete r.h. ranges. Maximum nitrate level resulting from HNO_3 (2.06 μmol/m^3) contamination in the NO_2/N_2 cylinder is indicated by the dashed line.

In Situ Measurement of Cloud Integrated Backscattering Coefficient with a Modified Nephelometer

T. Novakov, C. Rivera-Carpio, R.C. Schmidt, and C.F. Rogers

Clouds significantly affect the earth's radiation budget and are one of the principal sources of uncertainty in general circulation models. Reducing this uncertainty demands the improvement and validation of both cloud-radiation and cloud models based on observational data. Relevant cloud observations of both macroscopic and microscopic character are required. Toward this end we have initiated a field measurement program that focuses on the dependence of cloud reflective properties on atmospheric aerosol concentration, their chemical composition, and origin.

The field site is located at El Yunque peak (elevation 1067 m) in Puerto Rico, which is frequently in clouds and, depending on the air circulation pattern, exposed to aerosols of different compositions and origins. These may be natural (marine, Saharan dust) or anthropogenic (from surrounding islands or the continent). Because of this, the effects of these types of aerosols on cloud reflective properties can be conveniently studied.

In the initial phase of the project, we are measuring in-situ cloud drop number concentration and drop size distribution, liquid water content, and an optical property – the integrated backscattering coefficient, σ_{bs}, defined as

$$\sigma_{bs} = b\sigma_s$$

where b is the volume-averaged backscattering fraction and σ_s is the scattering coefficient, which depends on the drop size distribution, wavelength of light, complex index of refraction, and scattering efficiency. For optically thin clouds σ_{bs} is directly related to the cloud albedo for 0° zenith solar radiation A through the relation

$$A = \sigma_{bs} L$$

where L is the geometric thickness of the cloud. The backscattering coefficient σ_{bs} is therefore equal to the albedo per unit thickness of the cloud.

Cloud backscattering coefficients have been measured with a modified integrating nephelometer. A conventional nephelometer is designed for aerosol measurement and cannot be used in clouds because the cloud drops are retained in the inlet manifold so that only the interstitial aerosols are detected. To overcome these difficulties, we have modified a commercial nephelometer to provide for an open light-scattering volume so that cloud drops may freely pass. The instrument's performance is not affected by ambient daylight because the arrangement of the baffles and apertures does not allow direct sunlight to reach the photomultiplier. Values for the backscattering coefficient of clouds are of the order of 10^{-3}/m and therefore it is not required to operate the instrument at extreme sensitivity. We found that the background signal of the nephelometer in this mode of operation is essentially the same whether the scattering volume is closed or open. As done for aerosol measurements, the nephelometer is set to the backscattering mode of operation using a shutter blocking one-half the opal glass light source.

Examples of nephelometer strip chart recorded data obtained during different time periods of 1 August 1990 are shown in Figures 1 and 2. The variations of the nephelometer response seen in these figures reflect the horizontal inhomogeneities along the cloud traverse path, which for a 10-sec nephelometer time resolution corresponds to about 20 m. We note that the 10-sec variations in the nephelometer signal did closely track the 10-sec variations in the cloud drop concentrations, indicating that the cloud density at the CSASP

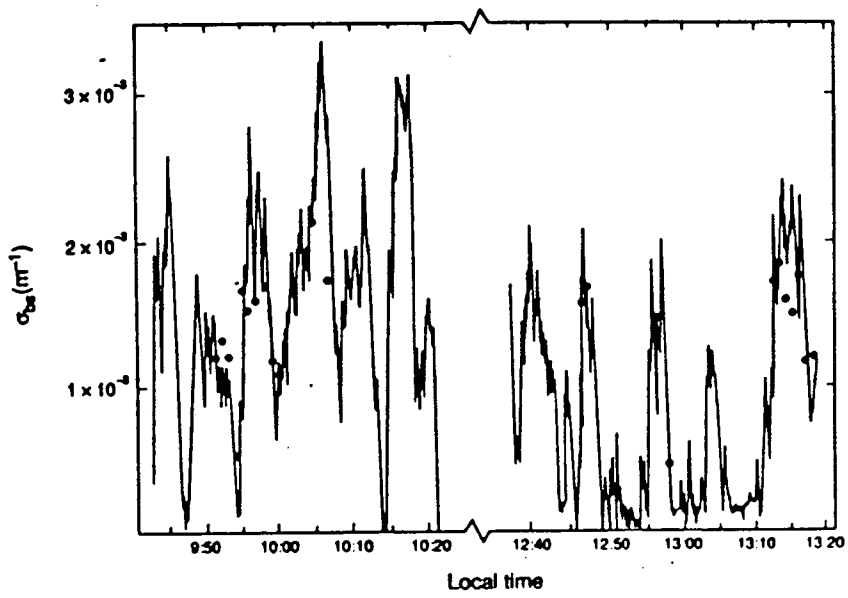

Figure 1. Measured σ_{bs} values plotted against local time (August 1, 1990). Theoretical values calculated from CASP (1-16 μm range) data are indicated by solid circles. (XBL 912-6433)

intake was essentially the same as in the nephelometer scattering volume.

The cloud drop number concentrations and size distributions obtained from CSASP measurements using the factory calibration were used to calculate (Mie theory) the σ_{bs} values for the wavelength of 0.55 μm. The calculated and measured σ_{bs} values are compared in Figure 1, where the calculated values are indicated by solid circles.

Calculated and measured σ_{bs} values are in good agreement, except at highback scattering values, when the calculated σ_{bs} is generally lower than measured. A possible explanation for this discrepancy is the presence of cloud drops with diameters greater than 16 μm, which the drop spectrometer did not record at the instrument range used (1-16 μm). This explanation is supported by the data shown in Figure 2 corresponding to a different time period when the CSASP was operated alternately in both the 1-16 and the 2-32 μm size ranges. Figure 2 shows that the agreement between measured and calculated σ_{bs} is indeed very good when the 2-32 μm range (open circles) rather than the 1-16 μm size range (solid circles) is used.

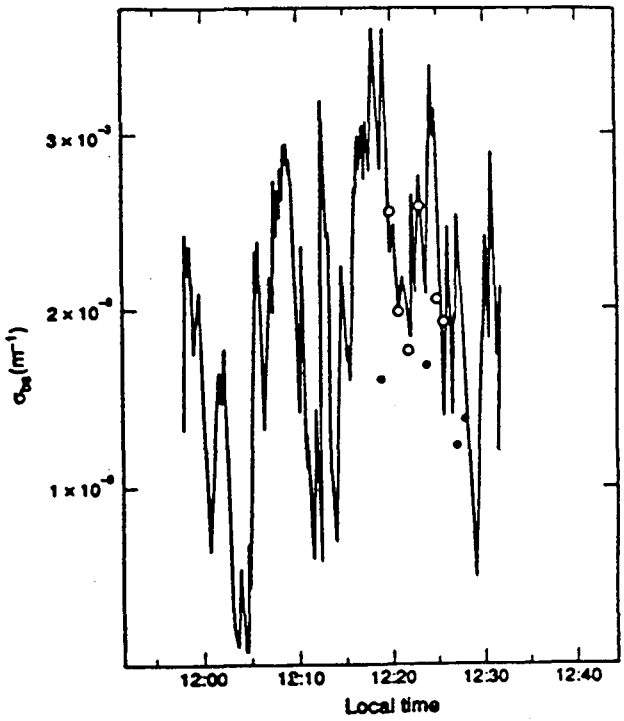

Figure 2. Measured σ_{bs} values for a different time period on August 1990. Theoretical values calculated from CSASP data for two size ranges, 1-16 μm (solid circles) and 2-32 μm (open circles). (XBL 912-6434)

Aerosol Particle Technology

Henry Benner

Tropospheric aerosol particles are customarily assigned a density because little is known about the actual density of individual particles. For tropospheric water droplets, density of 1 is reasonable but the density of windblown dust, pollen, agglomerated soot particles, and polar stratospheric cloud droplets is unknown. Particle density plays a role in the tropospheric lifetime of particles and the way in which they are collected by inertial samplers. Previously, we developed the capability to produce a beam of particles in vacuum; we are extending this technology to include the capability for determining particle density.

A polydisperse distribution of particles is first charged to a known and reproducible charge state so that particles of a specific diameter can be electrostatically separated from the initial population. These classified particles are drawn into a vacuum where a narrowly expanding particle beam is produced. As the charged particles pass between two capacitor plates, they are deflected away from the beam centerline. Their deflection is a simple function of their mass. Because the particles were first classified according to their diameter and then according to their mass, particle density can easily be calculated from their deflection distance. Of particular interest to aerosol scientists is the density distribution of submicron diameter particles because inaccuracies are introduced into density determinations when bulk properties are used as a basis for the density calculations. Density distributions of several types of particles are being determined. The procedure is also being extended to the determination of the properties, including density, of particles produced by the evaporation of solvent from solution droplets that contain DNA. This approach offers a new way to size DNA fragments that have been restricted by endonucleases, which would eliminate the need for time-consuming gel-electrophoresis separations.

MEMBRANE BIOENERGETICS

Free Radicals, Heavy Metal Toxicity, and Antioxidants

R.J. Mehlhorn, A.T. Mendez, K. Moore, T. Prolla, and M. Moronne

Free radicals (i.e., reactive molecules containing unpaired electrons) are produced in all aerobic organisms. Although elaborate defenses and repair systems have evolved to cope with free-radical damage, they are insufficient to prevent a gradual deterioration of functional integrity according to the "free-radical theory of aging." Understanding and ameliorating free-radical damage may prove to be the greatest accomplishment of modern biologists.

Our purpose is to elucidate mechanisms of free-radical damage. One hypothesis being tested is that iron released from heme proteins is a major free-radical catalyst. Because of its high iron content, the erythrocyte would then be a potential source of damage. This destructive potential could become expressed after traumatic injury or in a variety of blood diseases, including those associated with abnormal hemoglobins. Damage could be particularly severe when iron chelation, possibly by exogenous chelating agents from polluted air or water, has increased the iron-mediated free-radical production. To understand such chelation effects, we are studying the binding of heavy metal ions to components of cigarette smoke. We also seek to understand the fate of metal ion complexes that cannot be degraded by enzymic processes. This has let to an investigation of the accumulation of stable paramagnetic ion complexes in subcellular organelles, including efforts to link such complexes to ingested transition metal ions in marine organisms. To accomplish our research objectives, we have pioneered and are continuing to develop new methods to detect free radicals and to characterize the antioxidant systems that guard against them.

Our principal experimental approach is electron spin resonance (ESR), which detects magnetic moments presents in all free radicals. This basic approach is rendered highly sensitive with "free-radical traps," which accumulate adducts of free radicals until they are detectable by ESR. We are also developing a number of new methods for detecting and quantifying free iron, copper, and altered heme proteins.

Ascorbate Metabolism and Antioxidant Function in Erythrocytes

Our recent investigations of ascorbate regeneration in the human erythrocyte have revealed that treatment with hydroperoxides (tBH) and nitroxides transiently depletes cells of their ascorbate content and free-radical scavenging activity. We showed for the first time that two distinct free-radical reducing agents are related to vitamin C: 1) fully reduced ascorbic acid and 2) a product that arises from dehydroascorbic acid in the presence of thiols. Further, we showed that ascorbic acid is regenerated from dehydroascorbic acid (DHA) by a rapid mechanism at low DHA concentrations, whereas the chemical reduction of DHA by glutathione that is observed in buffer solutions becomes important only at higher DHA levels than are normally found in erythrocytes.

We used nitroxides to model persistent free radicals and to study free-radical quenching by ascorbate. Several equivalents of nitroxide were reduced relative to the ascorbate content of cells and transient oxidation of ascorbate by tBH and nitroxides did not inhibit subsequent nitroxide-reducing activity. We concluded that metabolically linked regeneration of ascorbate from DHA is an efficient process that allows ascorbate to function catalytically a a free-radical chain terminator. The reappearance of nitroxide reduction after tBH treatment and ascorbate oxidation indicated that the pentose phosphate pathway was not destroyed.

We also showed that ascorbate can be removed from erythrocytes by selective oxidation with cationic nitroxides without impairing the metabolic integrity of the cells. This procedure has made it possible for the first time to render cells ascorbate-deficient without prolonged nutritional manipulations.

Studies of Iron Chelates with Reduced Nitroxides

The one-electron oxidation of the reduced nitroxide 1,4-dihydroxy-2,2,6,6-tetramethyl-piperidine-N-Oxyl (TOLH) can be used to detect loosely bound iron. The rate of TOLH oxidation by Fe-EDTA in hemolysates is directly proportional to the iron chelate concentration. Sensitivity of this assay is in the submicromolar range. Preliminary experiments have shown that TOLH is not oxidized in hemolysates treated with EDTA, indicating that there is no detectable loosely bound iron in normal erythrocytes.

Development of Novel Antioxidants

Reduced nitroxides (TOLH) have the characteristics of ideal antioxidants. Like phenolic antioxidants, they readily donate hydrogen atoms to peroxyl radical without propagating chain reactions. Further, they are readily reduced by ascorbate and thus can be expected to persist in much the same way as ascorbate and tocopherol, both of which are now known to be metabolically regenerated after they function to terminate free-radical chain reactions. However, whereas physiological antioxidants are membrane-impermeable, many reduced nitroxides are highly permeable, which creates the possibility of introducing them into cells.

Production of Free Radicals by Thyroid Peroxidase

In the presence of hydrogen peroxide, peroxidase enzymes generate powerful oxidants *in vitro*. In the thyroid gland, oxidation of iodide by thyroid peroxidase iodinates the amino acid tyrosine as one of the steps in thyroid hormone synthesis. We have postulated that this enzyme may be a significant source of free radicals, particularly when the thyroid is exposed to high hydrogen peroxide loads—as may occur during inflammation—and in the presence of phenolic compounds, including species that may be ingested or inhaled. Using ESR measurements of the phenol-stimulated oxidation of TOLH, we have confirmed that a variety of phenolic molecules are oxidized to free radicals by thyroid peroxidase. We were gratified to observe that TOLH is also a powerful antioxidant that protects cultured thyroid cells from the lethality of phenols and hydrogen peroxide.

References

Mehlhorn RJ. Ascorbate- and dehydroascorbate-mediated reduction of free radicals in the human erythrocyte. *J. Biol. Chem.* (in press, 1990).

Mehlhorn RJ, Fuchs J, Sumida S, Packer L. Preparation of tocopheroxyl radicals for detection by ESR. *Methods in Enzymol.* 1990; 186: 197-205.

Fuchs J, Jurgen, Mehlhorn RJ, Packer L. Assay for free radical reductase activity in biological tissue by electron spin resonance spectroscopy. *Methods Enzymol.* 1990; 186: 670:674.

Moronne MM, Mehlhorn RJ, Miller MP, Ackerson LC, Macey RI. ESR measurement of time dependent and equilibrium volumes in red cells. *J. Membrane Biol.* 1990; 115: 31-40.

Prolla TA, Mehlhorn RJ. A photochemical system for generating free radicals: Superoxide, phenoxyl, ferryl and methyl. *Free Rad. Res. Commun.* 1990; 9: 135-146.

Biesert L, Adamski M, Zimmer G, Suhartono H, Fuchs J, Unkelbach U, Mehlhorn RJ, Hideg K, Milbradt R, Ruebsamen-Waigmann H. Anti-human immunodeficiency virus (HIV) drug HOE/BAY 946 increases membrane hydrophobicity of human lymphocytes and specifically suppresses HIV-protein synthesis. *Mid. Microbiol. Immunol.* 1990;179: 307-321.

Moore KL. Free radical generation by thyroid peroxidase and its effects on cells *in vitro*. Ph.D. Dissertation, University of California, Berkeley, 1990.

Biological Oxidations, Free Radicals, and Oxygen Toxicity

L. Packer, J. Maguire, V. Kagan, E. Serbinova, E. Witt, A. Reznick, M. Tsuchiya, and T.M. Forte

Our research strategy seeks to elucidate the interactions between oxidants and antioxidants in biological systems. The research has led to numerous publications and reports at national and international conferences. This past year, emphasis was given to three investigations:

Membrane Reactions of Vitamin E

Using ESR methods, we seek to identify sites, pathways, and specificity for vitamin E reactions by directly observing ascorbyl (vitamin C) and tocopheroxyl radicals. Our objectives are to learn about how vitamin E acts as the oxidant-harvesting center of biomembranes. Our studies suggest that the water- and lipid-soluble antioxidants present or electron transport components in membranes are "slaves" to vitamin E, donating their antioxidant potency to making vitamin E more efficient. HPLC and other methods are used to analyze factors that affect consumption of antioxidants such as vitamins E and C, and ubiquinones.

Lipoproteins

For human low-density lipoproteins (LDL), we are studying oxidative stress to LDL and analyzing antioxidant interactions and ways of minimizing oxidative damage to LDL.

Studies of UVAB-Exposed Skin

A solar simulator is used to expose skin of hairless mice to UVAB irradiation. We study the compromise of the skin antioxidant system and how to prevent loss of antioxidants, which leads to protein and lipid damage. Topical application of antioxidants or dietary interventions are used.

ECOLOGICAL SYSTEMS

Assessing Ecotoxicological and Genotoxic Effects in Environmental Management

S. Anderson, G. Wild, J. Harte

Genotoxic effects are an important consideration in ecological risk assessment. Substances which damage genetic material may cause decreased fertility, cancer, and multi-generational mutagenic effects. However, short-term genotoxicity tests, useful in multiple environmental media, have not been developed for wide application.

We have compared potential genotoxicity test systems using a number of well-characterized mutant strains of the nematode *Caenorhabditis elegans*. Dose-response curves for the mutagen ethyl methane sulfonate (EMS) were compared for two test systems. The spontaneous induction frequency was also analyzed. The first system, using the mutant strain *eT1* (Fig. 1), involved screening for recessive lethal mutations in a large region of the genome. The mutation frequency range, from 2-19 $\times 10^{-2}$, and 1000 animals can be tested and mutants detected and confirmed in 14 days. The second test system involved screening for recessive suppression of a nonmotile (*unc54*) mutant phenotype (Fig. 2). The mutation frequency ranged from 0.5-20 $\times 10^{-4}$ with 3 $\times 10^{-4}$ worms tested in 17 days. Therefore, in a relatively short period of time (12-17 days), genotoxic effects were detected and confirmed using both assay systems. These results indicate that varied sensitive approaches may be available for application of this unique genetic tool to environmental toxicology.

As test development has been completed, we are planning extensions of this work. We will further develop the assays for both the evaluation of genotoxic effects in environmental samples such as sediment and water, and the evaluation of genotoxic effects of environmentally significant chemicals. We are currently evaluating the metabolic activation potential of the nematode system and are evaluating methods for incorporating various metabolic activation systems.

Acute and chronic exposures of *C. elegans* to UV light have also been carried out, and effects have been noted at relatively low doses compared with sunlight. Chronic exposures utilizing varied wavelength distributions documented the dependence of mortality rates and reproductive success on wavelength. We are developing a system to study the effects of chronic exposures to natural sunlight enhanced with UV on *C. elegans* as well as selected aquatic species. The ultimate goal of our research on ultraviolet light is to model the potential multigenerational genotoxic effects of stratospheric ozone depletion.

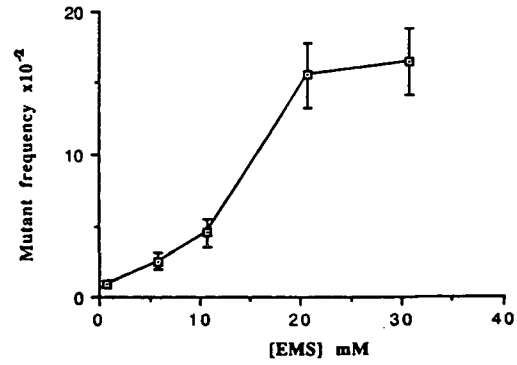

Figure 1. Results of *eT1* assay. Induced mutation frequency in JP10 strain following exposure to varying doses of EMS. 4 hr. exposure @21 C.

This year, a survey of ambient toxicity in marsh habitats of San Francisco Bay was also completed. Short-term indicators were used to evaluate potential effects of wastewater discharged into wetland habitats, and toxic effects were documented at selected sites. These studies have underlined the need for coupling engineering considerations with eco-

logical assessments at marshes managed to receive wastewater. Aspects of our project have been used to suggest criteria for toxicity characterization and remediation in wetlands.

References

Anderson SL, Hoffmann ER, Steward DS, Harte J. Ambient toxicity characterization of San Francisco Bay and adjacent wetland ecosystems. Lawrence Berkeley Laboratory Report No. LBL-29579, 1990.

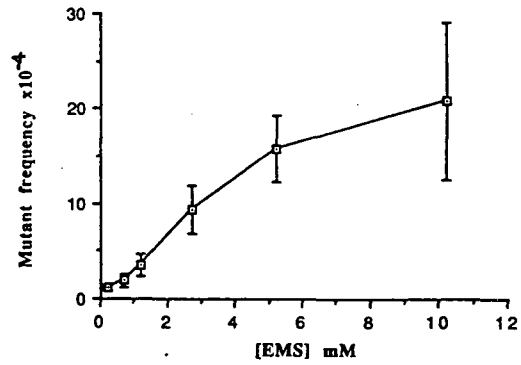

Figure 1. Results of *unc54* assay. Induced mutation frequency in TR1053 strain following exposure to varying doses of EMS. 4 hr. exposure @21 C.

Projects described in this report were supported by the following sources:

Director, Office of Energy Research:

Office of Basic Energy Sciences, Chemical Sciences Division

Office of Health and Environmental Research, Atmospheric and Climate Research Division

National Science Foundation under contract No. ATM-8914464.

NIH, by the Tobacco-Related Disease Research Program

LBL/JSU/AGMEF Science consortium

NIEHS Superfund Basic Research Program/UC Berkeley Program Project

California States Water Resources Control Board

This support was provided through the Department of Energy under Contract No. DE-AC03-76SF00098.

This document was prepared as an account of work sponsored by the United States Government. Neither the United States Government nor any agency thereof, nor The Regents of the University of California, nor any of their employees, makes any warranty, express or implied, or assumes any legal liability or responsibility for the accuracy, completeness, or usefulness of any information, apparatus, product, or process disclosed, or represents that its use would not infringe privately owned rights. Reference therein to any specific commercial product, process, or service by its trade name, trademark, manufacturer, or otherwise, does not necessarily constitute or imply its endorsement, recommendation, or favoring by the United States Government or any agency thereof, or The Regents of the University of California. The views and opinions of authors expressed herein do not necessarily state or reflect those of the United States Government or any agency thereof or The Regents of the University of California and shall not be used for advertising or product endorsement purposes.

Lawrence Berkeley Laboratory is an Equal Opportunity Employer

Applied Science Division
Lawrence Berkeley Laboratory
University of California
Berkeley, CA 94720